DRAFT IGTC2007-ABS-55

AERODYNAMIC INNER WORKINGS OF CIRCUMFERENTIAL GROOVES IN A TRANSONIC AXIAL COMPRESSOR

Chunill HAH[1], Martin MUELLER[2] and Heinz-Peter SCHIFFER[2]

[1]NASA Glenn Research Center,
MS 5-11, Cleveland, Ohio 44135
[2]Technische Universität Darmstadt
D-64287 Darmstadt, Germany

ABSTRACT

The current paper reports on investigations of the fundamental flow mechanisms of circumferential grooves applied to a transonic axial compressor. Experimental results show that the compressor stall margin is significantly improved with the current set of circumferential grooves. The primary focus of the current investigation is to advance understanding of basic flow mechanics behind the observed improvement of stall margin. Experimental data and numerical simulations of a circumferential groove were analyzed in detail to unlock the inner workings of the circumferential grooves in the current transonic compressor rotor. A short length scale stall inception occurs when a large flow blockage is built on the pressure side of the blade near the leading edge and incoming flow spills over to the adjacent blade passage due to this blockage. The current study reveals that a large portion of this blockage is created by the tip clearance flow originating from 20% to 50% chord of the blade from the leading edge. Tip clearance flows originating from the leading edge up to 20% chord form a tip clearance core vortex and this tip clearance core vortex travels radially inward. The tip clearance flows originating from 20% to 50% chord travels over this tip clearance core vortex and reaches to the pressure side. This part of tip clearance flow is of low momentum as it is coming from the casing boundary layer and the blade suction surface boundary layer. The circumferential grooves disturb this part of the tip clearance flow close to the casing. Consequently the buildup of the induced vortex and the blockage near the pressure side of the passage is reduced. This is the main mechanism of the circumferential grooves that delays the formation of blockage near the pressure side of the passage and delays the onset of short length scale stall inception. The primary effect of the circumferential grooves is preventing local blockage near the pressure side of the blade leading edge that directly determines flow spillage around the leading edge. The circumferential grooves do not necessarily reduce the over all blockage built up at the rotor tip section.

INTRODUCTION

A variety of casing treatments have been applied to extend the operating range of various compressors (Smith and Cumpsty [1984], Lee and Greitzer [1990], Moore et al. [1971], Prince et al. [1974], Fujita and Takata [1985], and Paulon and Dehoudt [1982]). Most previous experimental studies indicate that casing treatments, which are more effective in delaying stall, tend to induce additional loss at peak efficiency conditions.

Circumferential grooves on the compressor casing have been applied both for subsonic and transonic compressors. Although it is generally believed that the circumferential grooves on the compressor casing do suppress stall inception, the fundamental flow mechanisms are not well understood. Furthermore, the design criteria of the circumferential grooves are mainly based on loosely connected experimental data from subsonic compressors and their validity on transonic compressor is not clear. Most of the previous studies were aimed at obtaining the overall compressor performance data. No experimental studies to measure detailed flow features near the circumferential grooves have been reported.

With the advance of CFD technology, several attempts have been made to investigate the effects of casing treatments on compressor performance (Crook et al. [1995], Hall et al. [1994]). Paulon and Dehoudt [1982] conducted a theoretical investigation of the effects of circumferential grooves. Rabe and Hah [2002] investigated circumferential grooves applied to the first stage rotor in a modern highly loaded two-stage transonic axial compressor. They found that the local flow incidence near the pressure side of the

leading edge is reduced due to the circumferential grooves. Mueller et al. [2007] investigated various circumferential grooves applied to the rotor in a single stage transonic compressor.

The practical use of circumferential grooves is limited, like other casing treatments, because the quantitative physical mechanism is not understood clearly. They are very beneficial in most compressors although cases with no benefits have also been reported.

The purpose of the current investigation is to advance our understanding of the fundamental mechanisms of circumferential grooves on transonic compressor flow fields.

TEST ROTOR AND TEST FACILITY

Since 1994, the Chair of Gas Turbines and Aerospace Propulsion at Technische Universität Darmstadt has been operating an axial single-stage transonic compressor (see Figure 1).

The design parameters of the high-speed test rig represent a front stage of typical commercial HPCs. The rig has been built for validation of design tools and CFD codes. It also functions as an experimental test bed for new materials and manufacturing methods such as blisks and CRP. Until today, four different rotors have been tested. The test facility operates in an open circuit; ambient air is sucked into a settling chamber and through a calibrated bell mouth into the stage. Due to the length of the inlet duct and the small volume established at the stage outlet, stall can occur but surge cannot.

The rotor used for all measurements presented herein is the Darmstadt Rotor-1 titanium blisk with 16 radially stacked CDA-profiles. Table 1 shows the Rotor-1 geometries and the compressor characteristics at design conditions.

Probes inside the settling chamber were employed to identify the inlet flow conditions. For exit flow measurements, pressure and temperature rakes are mounted on the struts behind the stator. They are equipped with eleven radial sensors each. Therefore, all experimental results are related to the whole stage. Static wall pressure was measured at the same axial position as the rakes at hub and tip.

Four different casing inserts were manufactured, each representing another configuration of circumferential grooves. The groove onset downstream of the leading edge is at 15.25% of the projected axial chord. Details of the all the grooves are given by Mueller et al. [2007]. For the current study, the flow field with 6 deep grooves shown in Figure 2 is examined in detail.

NUMERICAL PROCEDURE

Steady and unsteady Reynolds-averaged Navier-Stokes (RANS) methods and a Large Eddy Simulation (LES) method were applied in the present study. The steady and unsteady three-dimensional RANS procedures were applied to obtain steady and unsteady flow fields at various operating conditions. The primary focus of the numerical analysis was to explain flow mechanism associated with the circumferential grooves. Therefore, the isolated rotor configuration with circumferential grooves was analyzed numerically. The current compressor stage has a relatively large space between the rotor and the stator, and the upstream influence of stator flow field on the rotor flow field is believed to be relatively minor. The unsteady RANS solutions were to obtain instantaneous flow structures during stall inception. A modified two-equation turbulence model was used for turbulence closure in the RANS methods. The LES procedure was applied primarily to explore additional unsteady flow features at near-stall operating conditions. With spatially filtered Navier-Stokes equations, the subgrid-scale stress tensor term must be modeled properly for closure of the governing equations. A Smagorinsky-type eddy-viscosity model was used for the subgrid stress tensor, and the standard dynamic model by Germano et al. [1991] was applied.

In the current study, the governing equations are solved with a pressure-based implicit method using a fully conservative control volume approach. A third-order accurate interpolation scheme is used for the discretization of convection terms and central differencing is used for the diffusion terms. The method is of second-order accuracy with smoothly varying grids. For the time-dependent terms, an implicit second-order scheme is used and a number of sub-iterations are performed at each time step. Details of the RANS method and applications to transonic flows are given by Hah and Wennerstrom [1991].

The computational grid for a single blade passage consists of 198 nodes in the blade-to-blade direction, 75 nodes in the spanwise direction, and 200 nodes in the streamwise direction. The inflow boundary was located 6 average blade heights upstream of the rotor leading edge and the outflow boundary was located one blade height from the trailing edge. The rotor tip clearance geometry is accurately represented by 28 nodes in the blade-to-blade direction, 16 nodes in the spanwise direction, and 140 nodes in the streamwise direction. The circumferential grooves were modeled in a separated block. Each groove is represented by 80 nodes in the circumferential direction and 20 nodes in the radial and axial directions. The I-grid topology is used to reduce grid skewness and a single-block grid is used. All the computations were performed with NASA's Columbia super computer system, which allows parallel computation with up to 512 computers.

Standard boundary conditions for an isolated rotor were applied at the boundaries of the computational domain. Circumferentially averaged static pressure at the casing was specified to control the mass flow rate. Non-reflecting boundary conditions were applied at the inlet and the exit boundaries.

OVERALL FLOW STRUCTURE

Measured compressor stage performance characteristics are given in Figures 3 and 4. Calculated rotor performance with and without circumferential grooves from the RANS calculation are also shown in Figures 3 and 4. The flow field without circumferential grooves at near-stall condition was also calculated with both single passage and full annulus

Large Eddy Simulation. The LES simulations were performed primarily to study unsteady nature of the flow.

The numerical simulations calculate slightly higher pressure rise than the measurement. With the numerical simulation, the stall mass flow rate was determined by increasing the exit reference pressure by a small increment until a stable converged solution could not be obtained. The numerical simulation calculated the stall point very close to the measured value for the smooth casing. For the grooved casing, the measurement shows almost 56% increase in the stall margin. On the other hand, the numerical simulation calculates about 45% increase in the stall margin. However, it seems that the numerical simulation calculates the extension of compressor stall margin clearly. Although the measurement shows that the adiabatic compressor stage efficiency is increased with the grooves, the numerical simulation shows the efficiency decreases slightly. Endwall flow separations near the stator blade have been observed for the current compressor stage at near-stall operation. It appears that the circumferential grooves decrease the endwall flow separations in the stator at near-stall operation, which results in the improvement of the overall efficiency of the stage. With the LES simulation, the time averaged pressure rise and the adiabatic efficiency were slightly lower than those from the RANS simulation. In the following sections, flow fields at near-stall condition are examined first. Then, flow fields with the six deep circumferential grooves are investigated in detail to delineate the flow mechanism of the circumferential grooves in the transonic compressor.

FLOW FIELD AT NEAR STALL OPERATION WITH SMOOTH CASING

Figure 5 compares changes in instantaneous endwall static pressure distributions from the measurement and the single passage LES calculation. Both the measurement and the calculation show large variation in both the shape and magnitude of the tip leakage core vortex. As the compressor operation moves toward the stall condition, the flow field becomes highly unsteady due to oscillations of the passage shock and the tip leakage vortex and interactions between them. Measured and calculated time-averaged static pressure contours on the casing are compared in Figure 6. The results in Figure 6 confirm that the overall flow structures are properly represented in the numerical simulation. The measurement and the calculation shown in Figures 5 and 6 are at the compressor operation just before short length scale stall inception occurs for the current compressor.

Velocity vectors near the leading edge at the rotor tip section from the time-averaged solution are shown in Figure 7. As indicated by previous studies (for example, Hah et al. [2004] and Vo et al. [2005]), there is no flow spillage to the adjacent blade passage at the leading edge at this operating condition.

Detailed flow structures inside the tip gap are illustrated with particle traces from the middle of the tip gap in Figure 8. As observed in other transonic compressors (Hah et al. [2004]), the core tip leakage vortex (black traces in Figure 8) is formed by the flow particles coming over the tip gap between the leading edge and about 20% blade chord. As this tip core vortex travels down the passages, it moves radially inward. Flow particles from the tip gap between 20% and about 50% blade chord from the leading edge (red traces in Figure 8) flow over the tip clearance core vortex and accumulate near the pressure side of the leading edge of the adjacent blade, forming the induced vortex. The formation of the induced vortex and its influence on tip clearance flow in a transonic compressor were also previously studied by Van Zante et al. [2000].

Entropy generation at the rotor tip section is shown in Figure 9. Strong flow blockage is seen to form near the pressure side of the leading edge. Particle traces shown in Figure 8 indicate that tip clearance flows which come over the tip clearance core vortex with lower momentum contribute a large portion of this blockage. The tip clearance core vortex shown as black traces in Figure 8 does not exhibit so-called vortex breakup at this operating condition. As the core vortex expands downstream, it creates additional blockage in the passage. However, it does not seem that core vortex breakup leads directly to stall inception for the current compressor. As the mass flow rate is decreased further, flow spillage occurs near the leading edge and short length scale stall inception occurs.

Figure 10 shows particle traces at the rotor tip just after stall inception occurs. A much stronger induced vortex is observed as the flow rate decreases while tip core vortex breakup occurs. Results in Figures 7 through 10 show that the induced vortex plays a key role in the buildup of blockage and short length scale stall inception.

Figure 11 shows the instantaneous Mach number distribution over the stalled and healthy blade passages at near-stall operation from a full annulus flow simulation. A strong induced vortex is observed when a blade passage is stalled. Again, results from full annulus flow simulation, which is more realistic, support that the induced vortex directly influences the buildup of blockage and short length scale stall inception.

INFLUENCE OF THE CIRCUMFERENTIAL GROOVES ON THE TIP CLEARANCE FLOW AND STALL INCEPTION

Both the measurement and the numerical simulation show that the circumferential grooves increase the stall margin of the current compressor. The measurements have shown varying degrees of improvement in stall margin for different configurations of the grooves. To investigate the flow mechanism behind the stall margin improvement with the grooves, numerical simulations with six deep grooves were examined. As the grooves are installed on the casing, it is believed that flow field close to the casing is influenced most by the grooves.

As shown in Figures 3 and 4, numerical simulation shows that six deep grooves delay stall inception beyond the mass flow rate of 14 kg/sec where stall inception occurs with the smooth casing. To study changes in the flow field near the casing by the grooves, the flow field at 14 kg/sec with

the six deep grooves is analyzed and compared with that at the same flow rate with the smooth casing.

Figure 12 shows calculated velocity vectors in the grooves near the suction side of the blade. As expected, the two front grooves have a larger influence over the flow field where the pressure gradient across the blade tip is high and the induced vortex originates.

Calculated velocity vectors near the tip and just below casing are shown in Figure 13. Compared to the flow field with the smooth casing, the velocity vectors show that the flow field with the grooves has less of a negative axial velocity component.

Particle traces from the rotor tip at the middle of the tip clearance are shown in Figure 14. Particle traces in Figure 14 show that the tip core vortex is not influenced directly by the circumferential grooves as it moves radially inward and downstream. However, flow between the core vortex and the casing is altered drastically by the circumferential grooves. Tip clearance flows originating from the blade tip gap between 20% and 50% chord from the leading edge do not reach to the area near the pressure side of the leading edge where the high blockage occurs. Instead these flows merge around the tip clearance core vortex. Consequently, less loss accumulates near the pressure side of the leading edge, which delays flow spillage and short length scale stall inception.

This change of flow pattern close to the casing occurs due to several effects by the grooves. First, the pressure gradient across rotor tip below the grooves is reduced due to the groove. Radial flow into and out of the grooves shown in Figure 12 also reduces circumferential movement of the tip clearance flows beneath the grooves. Entropy contours at the blade tip with the six deep grooves are shown in Figure 15. The entropy contours in Figure 15 confirm that less loss accumulates near the pressure side of the leading edge. The numerical simulation shows that the total mass flow rate going through the tip gap is reduced about 60% with the six deep grooves at this operating condition compared to the smooth casing.

CONCLUDING REMARKS

The effects of casing circumferential grooves on the stall margin of a transonic compressor rotor were studied with the measured data and numerical simulation of the flow field. Detailed examination of the numerical simulation of the flow fields with and without casing grooves reveals following.

1. An induced vortex is created near the pressure side of the leading edge as the compressor operates at the near-stall condition. This region is formed by the tip clearance flows that originate from the tip gap between 20% and 50% of the blade chord and represents a high blockage area. Short length scale stall inception occurs as this blockage increases, which results in flow spillage around the leading edge into the adjacent blade passage.
2. Circumferential grooves diminish the circumferential movement of the tip clearance flow. Tip clearance flow from 20% to 50% chord of the blade does not reach the pressure side of the leading edge. This is due to reduced pressure gradient under the grooves and radial suction and injection of the flows near the grooves. The circumferential grooves do not necessarily reduce the overall generation of loss. Rather, the grooves redistribute the aerodynamic loss in the tip clearance region.

ACKNOWLEDGMENTS

The authors would like to acknowledge the contribution of J. Loellbach of ICOMP during the current investigation.

REFERENCES

Crook, A. J., Greitzer, E. M., Tan, C. S., and Adamczyk, J. J., 1993, "Numerical Simulation of Compressor Endwall and Casing Treatment Flow Phenomena," ASME Journal of Turbomachinery, Vol.115, No.3, pp.501-512.

Fujita, H. and Takata, H., 1985, "A Study of Configurations of Casing Treatment for Axial Flow Compressors," Bull. of JSME, Vol. 27, No. 230, pp. 1675-1681.

Germano, M., Piomelli, U., Moin, P., and Cabot, W. H., 1991, “A Dynamic Subgrid-Scale Eddy-Viscosity Model,” Journal of Fluid Mechanics, Vol. A3, pp. 170-176.

Hah, C., Rabe, D. C., and Wadia, A. R., 2004, "Role of Tip-Leakage Vortices and Passage Shock in Stall Inception in a Swept Transonic Compressor Rotor," ASME Paper GT2004-53867.

Hah, C. and Wennerstrom, A. J., 1990, "Three-Dimensional Flow Fields Inside a Transonic Compressor with Swept Blades," ASME Journal of Turbomachinery, Vol. 113.,No. 1, pp. 241-251.

Hall, E. J., Heidegger, N. J., and Delaney, R. A., 1996, "Performance Prediction of Endwall Treated Fan Rotors with Inlet Distortion," AIAA Paper AIAA 96-0244.

Lee, N. K. W. and Greitzer, E. M., 1990, "Effects of Endwall Suction and Blowing on Compressor Stability Enhancement", ASME Journal of Turbomachinery, Vol. 122, pp. 133-144.

Moore, R. D., Kovich, G., and Blade, R. J., 1971, "Effect of Casing Treatment on Overall and Blade-Element Performance of a Compressor Rotor", NASA TN D-6538.

Mueller, M. W., Schiffer, H. P., and Hah, C., 2007, “Effects of Circumferential Grooves on the Aerodynamic Performance of an Axial Single-Stage Transonic Compressor,” ASME Paper GT-2007-27365.

Paulon, J. and Dehondt, D., 1982, "Influence of Casing Treatment on the Operating Range of Axial Compressors," ASME Paper 82-GT-103.

Prince, D. C., Jr., Wisler, D. C., and Hilvers, D. E., 1974, "Study of Casing Treatment Stall Margin Improvement Phenomena," NASA CR-134552.

Rabe, D. C. and Hah, C., 2002, “Application of Casing Circumferential Grooves for Improved Stall Margin in a Transonic Axial Compressor,” ASME Paper GT-2002-30641.

Smith, G. D. J. and Cumpsty. N. A., 1985, "Flow Phenomena in Compressor Casing Treatment", ASME Journal of Engineering for Gas Turbines and Power, Vol. 117, pp. 532-541

Van Zante, D. E., Strazisar, A. J., Wood, J. R., Hathaway, M. D., and Okiishi, T. H., 2000, "Recommendations for Achieving Accurate Numerical Simulation of the Tip Clearance Flows in Transonic Compressor Rotors," ASME Journal of Turbomachinery, Vol. 122, pp. 733-742.

Vo, H. D., Tan, C. S., and Greitzer, E. M., 2005, "Criteria for Spike Initiated Rotating Stall," ASME Paper GT2005-68374.

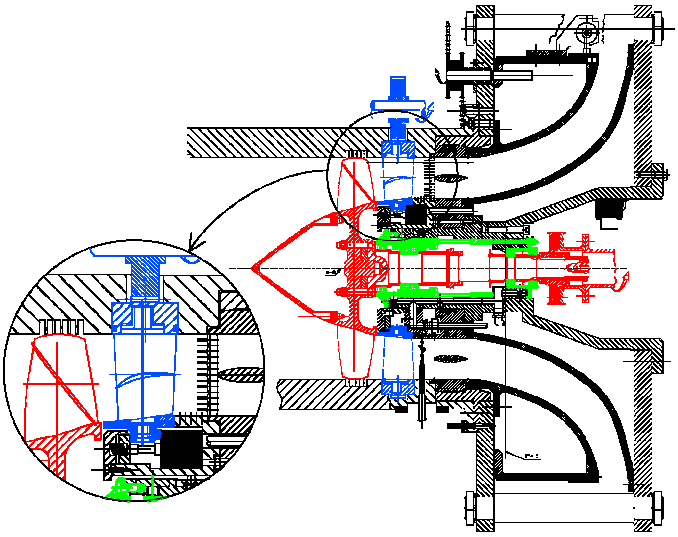

Figure 1: Cross section of transonic compressor stage with circumferential casing grooves.

Pressure ratio	1.5
Corrected mass flow rate	16.0 kg/s
Corrected tip speed	398 m/s
Inlet relative Mach number at tip	1.35
Inlet relative Mach number at hub	0.70
Shaft speed	20,000 rpm
Tip diameter	0.38 m
Rotor mean aspect ratio	0.94
Rotor solidity (hub/mid/tip)	1.9/1.5/1.2

Table 1 Rotor design parameters.

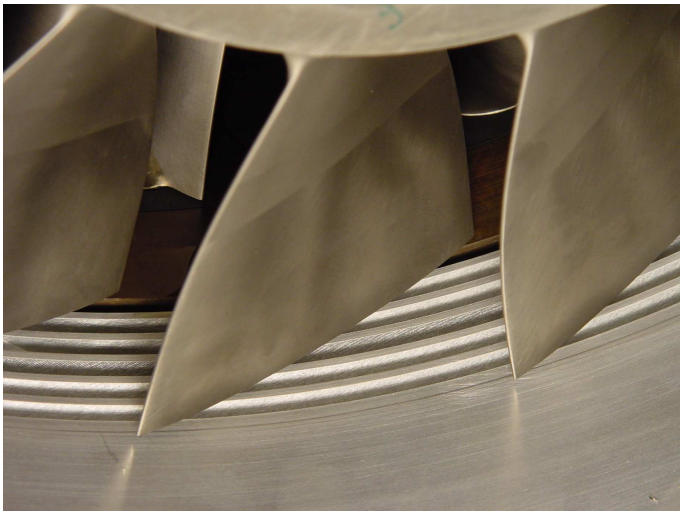

Figure 2: Compressor rotor with six deep grooves.

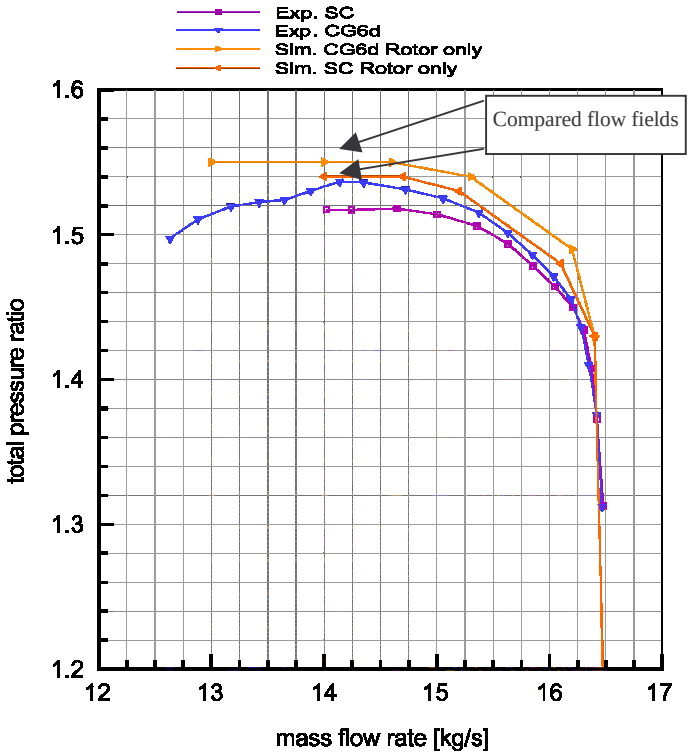

Figure 3: Total pressure rise at design speed.

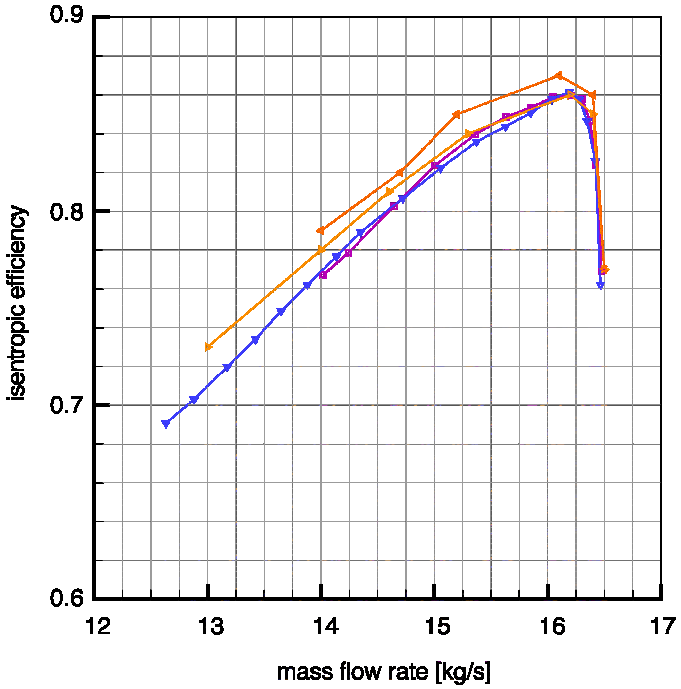

Figure 4: Isentropic efficiency at design speed.

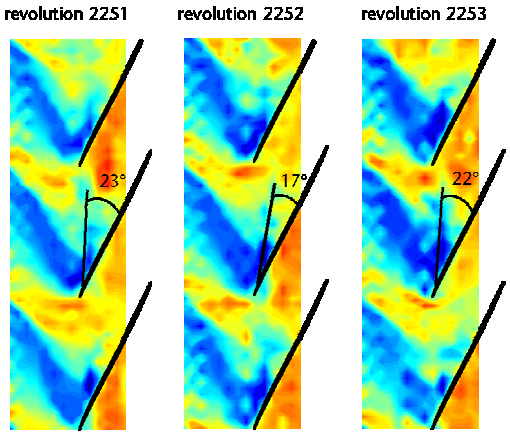

Figure 5 a.: Measured instantaneous endwall static pressure distributions near stall.

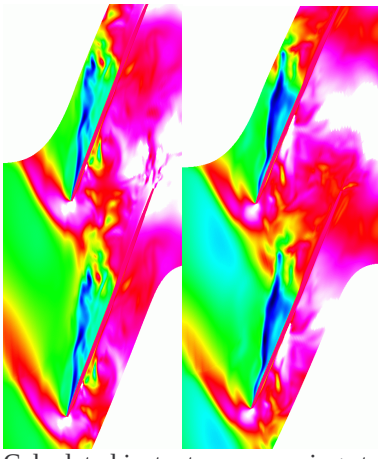

Figure 5 b: Calculated instantaneous casing static pressure from LES near stall.

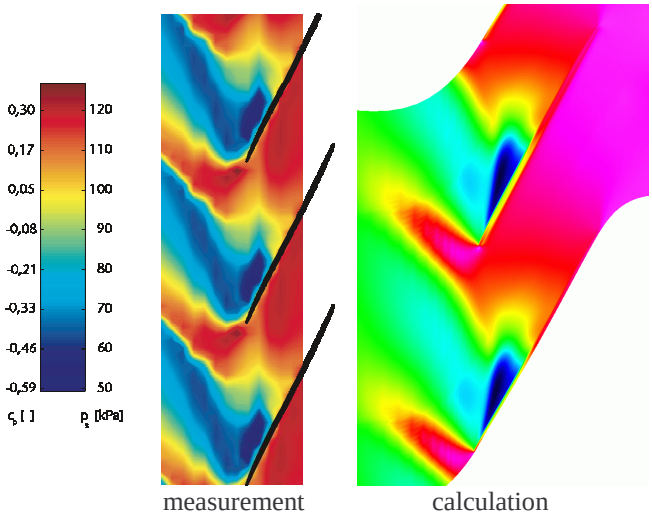

Figure 6: Comparison of casing static pressure distribution near stall.

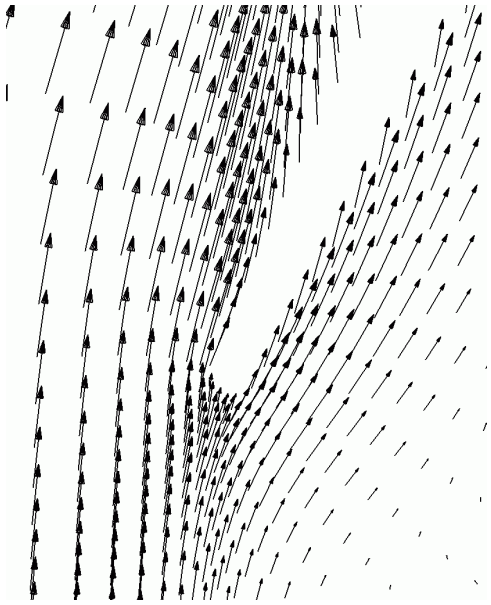

Figure 7: Velocity vectors at rotor tip, near stall.

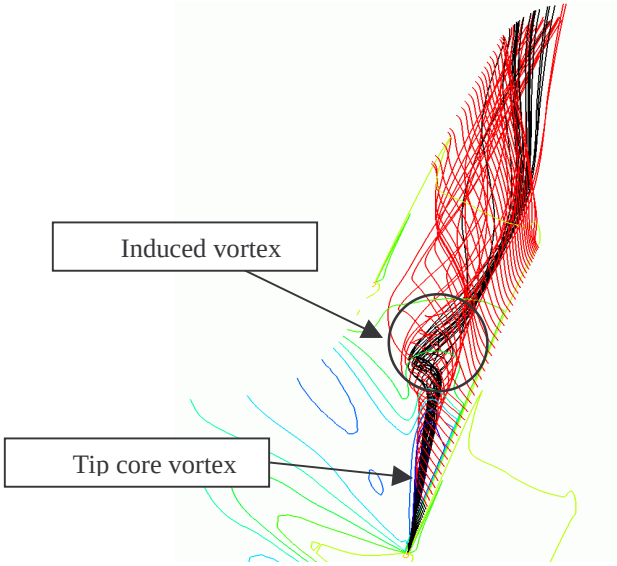

Figure 8: Particle traces from the middle of the tip gap.

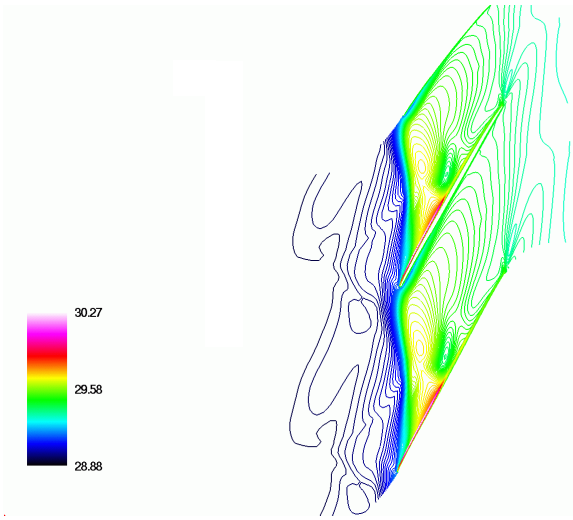

Figure 9: Entropy contours at the blade tip, near stall

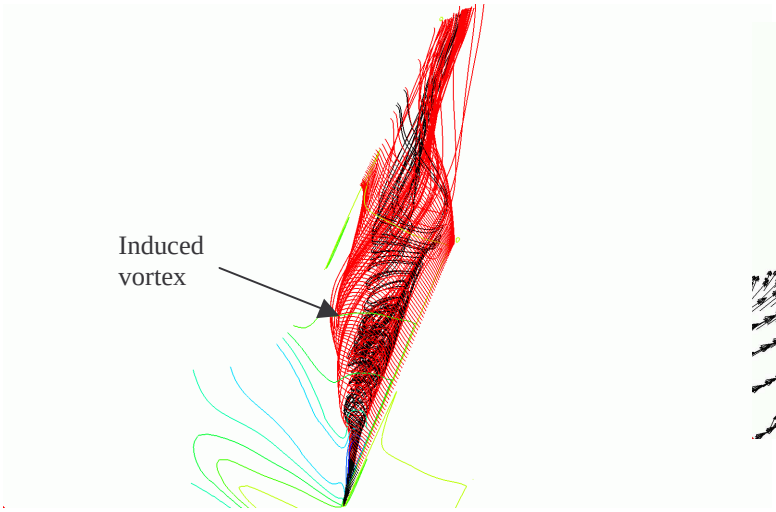

Figure 10: Particle traces from the middle of the tip gap, smooth wall and after stall inception.

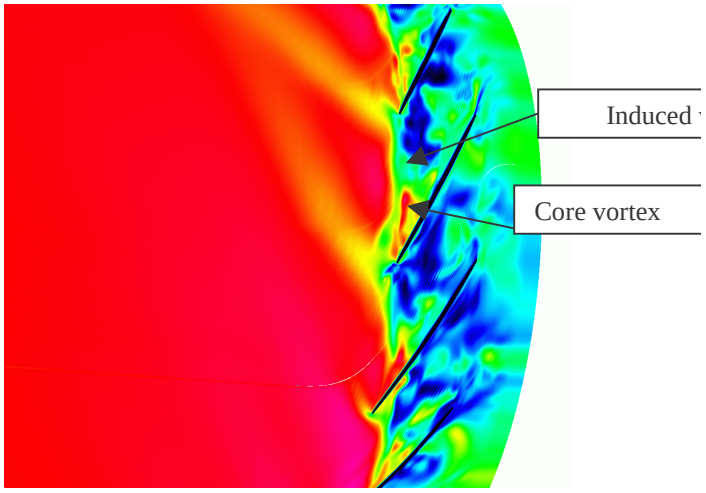

Figure 11a: Instantaneous Mach number contours at rotor tip across blade passages with large induced vortex, near stall.

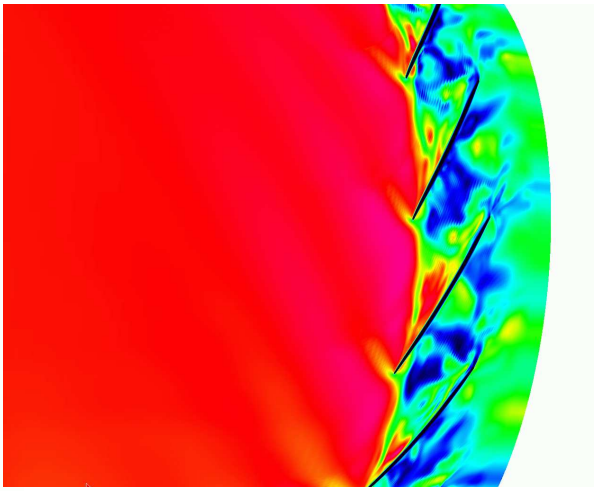

Figure 11 b: Instantaneous Mach number distribution at rotor tip across blade passages with smaller induced vortex, near stall.

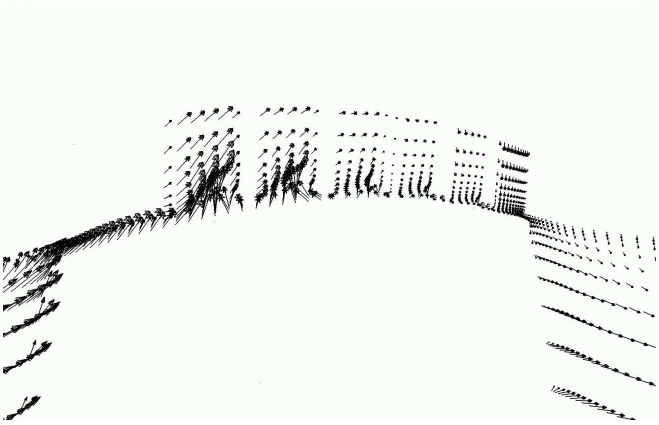

Figure 12: Velocity vectors inside grooves, 14Kg/s.

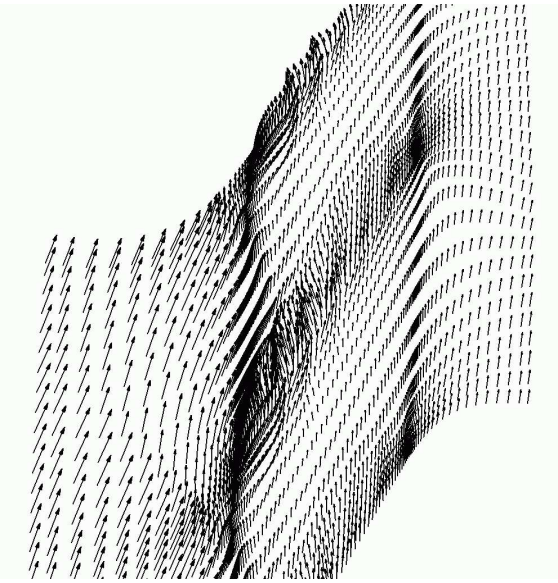

Figure 13 : Velocity vectors at the middle of tip gap section, 6 deep grooves, 14 Kg/s.

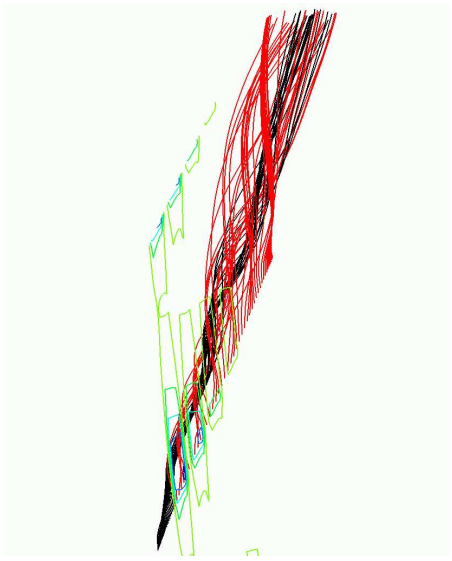

Figure 14 : Particle traces from the middle of tip gap with 6 deep grooves, 14Kg/s.

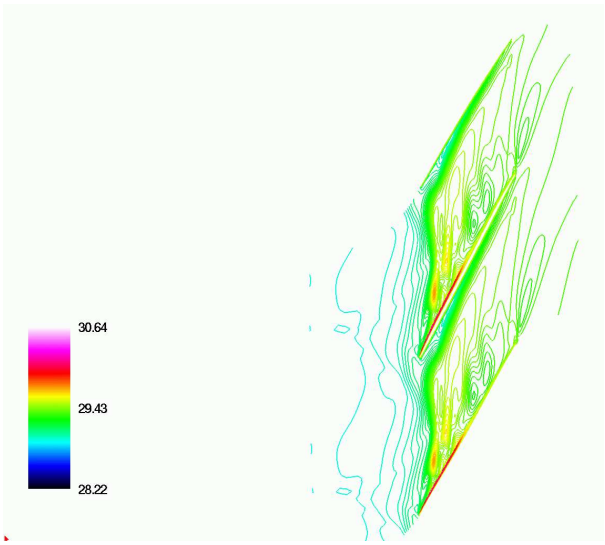

Figure 15 : Entropy contours at the blade tip with 6 deep grooves, 14 Kg/s.